DTNSRDC-82/036

PREDICTED MOTIONS OF HIGH-SPEED SWATH SHIPS IN HEAD AND FOLLOWING SEAS

DAVID W. TAYLOR NAVAL SHIP RESEARCH AND DEVELOPMENT CENTER

Bethesda, Maryland 20084

PREDICTED MOTIONS OF HIGH-SPEED SWATH SHIPS IN HEAD AND FOLLOWING SEAS

by

Young S. Hong

APPROVED FOR PUBLIC RELEASE: DISTRIBUTION UNLIMITED

SHIP PERFORMANCE DEPARTMENT
RESEARCH AND DEVELOPMENT REPORT

July 1982 DTNSRDC-82/036

MAJOR DTNSRDC ORGANIZATIONAL COMPONENTS

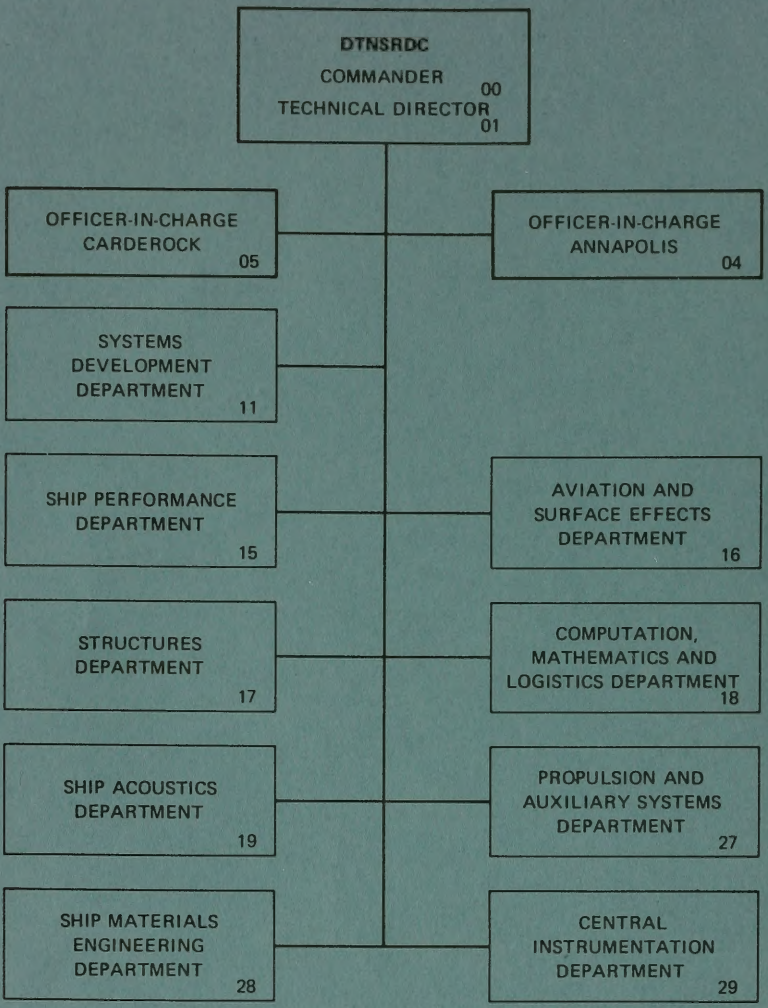

GPO 866 993

REPORT DOCUMENTATION PAGE

READ INSTRUCTIONS BEFORE COMPLETING FORM

1. REPORT NUMBER: DTNSRDC-82/036

2. GOVT ACCESSION NO.

3. RECIPIENT'S CATALOG NUMBER

4. TITLE (and Subtitle)

PREDICTED MOTIONS OF HIGH-SPEED SWATH SHIPS IN HEAD AND FOLLOWING SEAS

5. TYPE OF REPORT & PERIOD COVERED: Final

6. PERFORMING ORG. REPORT NUMBER

7. AUTHOR(s)

Young S. Hong

8. CONTRACT OR GRANT NUMBER(s)

9. PERFORMING ORGANIZATION NAME AND ADDRESS

David W. Taylor Naval Ship Research and Development Center
Bethesda, Maryland 20084

10. PROGRAM ELEMENT, PROJECT, TASK AREA & WORK UNIT NUMBERS

(See reverse side)

11. CONTROLLING OFFICE NAME AND ADDRESS

Naval Sea Systems Command
Washington, D.C. 20362

12. REPORT DATE: July 1982

13. NUMBER OF PAGES: 52

14. MONITORING AGENCY NAME & ADDRESS(if different from Controlling Office)

15. SECURITY CLASS. (of this report): UNCLASSIFIED

15a. DECLASSIFICATION/DOWNGRADING SCHEDULE

16. DISTRIBUTION STATEMENT (of this Report)

APPROVED FOR PUBLIC RELEASE: DISTRIBUTION UNLIMITED

17. DISTRIBUTION STATEMENT (of the abstract entered in Block 20, if different from Report)

18. SUPPLEMENTARY NOTES

19. KEY WORDS (Continue on reverse side if necessary and identify by block number)

Small-Waterplane-Area Twin-Hull (SWATH) Ship
Heave Motion, Pitch Motion
Following Seas
Head Seas
High Speed
Unified Slender-Body Theory
Strip Theory

20. ABSTRACT (Continue on reverse side if necessary and identify by block number)

Unified slender-body theory has been applied to predicting the motion of small-waterplane-area twin-hull high-speed (SWATH) ships in head seas. Using this theory, numerical results indicate an improvement in accurately predicting the effects of added-mass and damping coefficients when compared with strip theory. However, the same improvement is not achieved in predicting the effects of exciting forces and motions. Corrections in

(Continued on reverse side)

(Block 10)

Program Element 61153N
Task Area SR 0230101
Work Unit 1572-031

(Block 20 continued)

the numerical computation of previous work have been implemented; previous calculations for following seas have also been repeated. The pitch motions of SWATH 6D in following seas are now in good agreement with the results of scale model experiments. However, the motion results of SWATH 6A in following seas show large unexplained peak values when the encounter frequency becomes very small.

TABLE OF CONTENTS

LIST OF FIGURES

LIST OF TABLES

MATHEMATICAL NOTATION AND CONSTANTS

A	Amplitude of incoming wave
A_{jk}	Added-mass coefficients (j, k=3 for heave; j, k=5 for pitch)
B_{jk}	Damping coefficients (j, k=3 for heave; j, k=5 for pitch)
C_j	Coefficient for longitudinal interaction
C_{jk}	Hydrostatic coefficients
D	Displacement of SWATH ship
$\overline{D}$	Pitch determinant
F_i	Heave exciting force (i=3) or pitch exciting moment (i=5)
G	Green function
g	Gravitational acceleration
H_i	Heave (i=3) and pitch (i=5) amplitudes
I	Mass moment of inertia
$i = (-1)^{1/2}$	Imaginary unit
$K = \omega^2/g$	Wave number of frequency of encounter (also, $K_o = \omega_o^2/g$ is the incoming wave number)
L	Characteristic length of SWATH ship
M	Mass of SWATH ship
$\vec{m}(m_1,m_2,m_3)$	Normal vector due to the steady forward potential
$m = U^2/g$	A constant
$\vec{n}(n_1,n_2,n_3)$	Unit vector directed normal into the fluid
$O(x,y,z)$; $O(\xi,\eta,\zeta)$	Coordinate systems with origin at O
p	Pressure

q	Three-dimensional source strength
S	Area of immersed cross section
$\vec{U}_o(-U,0,0)$	Steady forward velocity vector
x,y,z	Spatial coordinates
α_m	Multipole strength
β	Heading angle of incoming wave with respect to the x axis (β = 0° is the following wave, and β = 180° is the head wave)
$\gamma = 0.57721...$	Euler's constant
λ	Length of incoming wave
ξ,η,ζ	Spatial coordinates
ξ_j	Complex amplitude of ship motion
σ_j	Two-dimensional source strength
$\phi\left(=\sum_i \phi_i = \phi_1 + \phi_2\right)$	Total velocity potential
ϕ_i	Velocity potential due to steady forward motion (i=1) or to unsteady oscillations (i=2)
ϕ_j, j = 3,5	Two-dimensional velocity potential for heave (j=3) or pitch (j=5) due to harmonic motion
$\hat{\phi}_j$, j = 3,5	Two-dimensional velocity potential for heave (j=3) or pitch (j=5) due to steady forward motion
ω	Encounter frequency
ω_o	Frequency of incoming wave
φ_o	Incoming wave potential
φ_j(j=1,2,...,6)	Velocity potential due to motion of the ship with unit amplitude in each of six degrees of freedom
φ_7	Diffraction potential

ABBREVIATIONS AND UNITS OF MEASUREMENT

GM	Metacentric height
kg	Kilogram
m	Meter
PV	Principal value
sec	Second
SWATH	Small-waterplane-area twin-hull

ABSTRACT

Unified slender-body theory has been applied to predicting the motion of small-waterplane-area twin-hull high-speed (SWATH) ships in head seas. Using this theory, numerical results indicate an improvement in accurately predicting the effects of added-mass and damping coefficients when compared with strip theory. However, the same improvement is not achieved in predicting the effects of exciting forces and motions. Corrections in the numerical computation of previous work have been implemented; previous calculations for following seas have also been repeated. The pitch motions of SWATH 6D in following seas are now in good agreement with the results of scale model experiments. However, the motion results of SWATH 6A in following seas show large unexplained peak values when the encounter frequency becomes very small.

ADMINISTRATIVE INFORMATION

This work was performed under the General Hydromechanics Research Program administered by the DTNSRDC Ship Performance Department and was authorized by the Naval Sea Systems Command, Hull Research and Technology Office. Funding was provided under Program Element 61153N, Task Area SR 0230101, and Work Unit 1572-031.

INTRODUCTION

An analytical method for predicting the motions of small-waterplane-area twin-hull (SWATH) ships has been developed using the strip theory developed earlier by Lee.[1*] The method has been further improved for the computation of heave and pitch motions in head seas by adding the surge effect on the pitch exciting moment and by correcting the viscous-damping terms developed by the present author.[2] The numerical results correlate well with experimental results for a moderate speed range.

The original strip theory has several limitations in application. First, when the encounter frequency is very small, strip theory cannot be properly applied. The small encounter frequency occurs when a ship proceeds with a fairly high speed in following seas. Second, the strip theory does not predict the motion correctly when a ship moves at high speed in head seas. The fundamental assumption of the strip theory is that the encounter frequency should be far larger than the longitudinal gradient of the body surface multiplied by the forward speed.[3]

*A complete listing of references is given on page 41.

Newman[4] recently applied slender-body theory to the problem of predicting ship motion. He has developed a unified slender-body theory and applied it to the computation of added-mass and damping coefficients. Newman and Sclavounos[5] have computed added-mass and damping coefficients for surface ships, and their numerical results agree well with the three-dimensional results for a surface ship when the forward speed is zero. For the case of nonzero forward speed, the agreement is not as good as for zero speed.

The author has previously applied the unified slender-body theory to the computation of motions of SWATH ships in following seas.[6] This resulted in an improvement in predicting the effects of added-mass and damping coefficients, but a rather inconsistent improvement in motion predictions. Furthermore, the numerical handling of the hydrodynamic singularity was deficient; this singularity problem has been corrected. Numerical computations in following seas are repeated in this report.

The unified slender-body theory is here applied to improve the prediction of motion of high-speed SWATH ships in head seas. Two-dimensional theory is applied in the inner region and three-dimensional theory is applied in the outer region of the hydrodynamic flow domain. The matching process is taken in an intermediate region, and the correction terms are added to the results of the strip theory. The numerical results are compared with those of strip theory and experiment. An improvement in predicting hydrodynamic coefficients has been achieved, but a similar improvement has not been obtained in the motion results.

EQUATIONS OF MOTION

COORDINATE SYSTEMS

Two coordinate systems are defined: the first $O_o(x_o,y_o,z_o)$ is fixed in space, and the second $O(x,y,z)$ is fixed with respect to the ship which moves with a forward speed U along the positive $O_o x_o$ axis. The Oz axis is directed vertically upward, and the Ox axis is positive in the direction of the ship's forward velocity (Figure 1). The Oxy-plane is in the plane of the undisturbed free surface. The two coordinate systems coincide when the ship is at rest at time zero.

Using the slender-body theory, the length of the ship is assumed to be far larger than the beam or the draft. We separate the fluid domain (y,z) into two regions: the outer region where (y,z) is of the order of the length of the ship, and the inner region where (y,z) is of the order of the beam or draft. In the outer

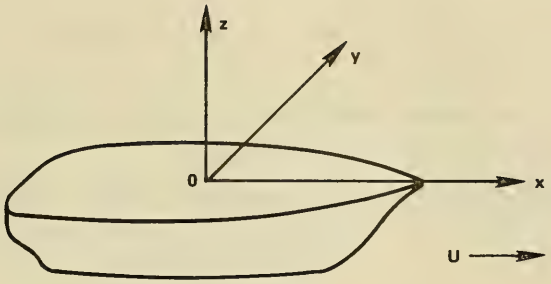

Figure 1 - Coordinate System Fixed with Respect to the Ship. This System Moves with a Speed U Relative to a System Fixed in Space

region, the three-dimensional Laplace equation is solved under a three-dimensional free-surface condition and an imposed radiation condition. The inner solution is governed by the two-dimensional Laplace equation with two-dimensional boundary conditions. These two solutions are matched in the overlapping domain or intermediate region to determine the solution of the unified slender-body theory.

The governing equations of velocity potentials, boundary conditions, and their solutions will now be given. The details of the derivations are given in References 4 and 6.

POTENTIAL OF STEADY FORWARD MOTION

The velocity potential of steady forward motion can be expressed as

$$\phi_1(x,y,z) = - U\, x + \phi_o(x,y,z) \tag{1}$$

where $\phi_o(x,y,z)$ satisfies Laplace's equation and the free surface and body boundary conditions given by

$$\phi_{oxx} + \phi_{oyy} + \phi_{ozz} = 0 \qquad z < 0 \tag{2}$$

$$(U^2/g)\, \phi_{oxx} + \phi_{oz} = 0 \qquad z = 0 \tag{3}$$

$$(\nabla\phi_o + \vec{U}_o) \cdot \vec{n} = 0 \qquad \text{on the body surface} \tag{4}$$

Here $\vec{U}_o$ (-U,0,0) is the steady forward velocity vector, and $\vec{n}$ is the unit normal vector of the body directed into the fluid domain.

The solution of Equations (2)-(4) is given by Tuck[7] as

$$\phi_1 = \frac{a}{2} \log \bar{r} + \frac{a}{2} \log \bar{r}_1 - U x \tag{5}$$

where $a = \frac{U}{\pi} S'$ = the strength of the source

S = area of the immersed cross section

$S' \equiv dS/dx$

$$\bar{r} = [(y-\eta)^2+(z-\zeta)^2]^{1/2}$$

and

$$\bar{r}_1 = [(y-\eta)^2+(z+\zeta)^2]^{1/2}$$

Here, (y,z) is the point where the potential is solved and (η,ζ) is the source point.

TWO-DIMENSIONAL POTENTIAL OF OSCILLATION

The two-dimensional velocity potential due to pure heave oscillation is given by

$$\varphi_3^{(S)} = \phi_3 + \hat{\phi}_3 \tag{6}$$

The first potential satisfies the following conditions

$$\frac{\partial^2\phi_3}{\partial y^2} + \frac{\partial^2\phi_3}{\partial z^2} = 0 \qquad \text{when } z < 0 \tag{7}$$

$$\frac{\partial\phi_3}{\partial z} - \frac{\omega^2}{g}\phi_3 = 0 \qquad \text{on } z = 0 \tag{8}$$

and

$$\frac{\partial \phi_3}{\partial n} = - i \omega n_3 \qquad \text{on the body surface} \tag{9}$$

n_3 is the heave component of the unit vector $\vec{n}$. The second potential of Equation (6) satisfies the following conditions:

$$\frac{\partial^2 \hat{\phi}_3}{\partial y^2} + \frac{\partial^2 \hat{\phi}_3}{\partial z^2} = 0 \qquad \text{when } z < 0 \tag{10}$$

$$\frac{\partial \hat{\phi}_3}{\partial z} - \frac{\omega^2}{g} \hat{\phi}_3 = 0 \qquad \text{on } z = 0 \tag{11}$$

and

$$\frac{\partial \hat{\phi}_3}{\partial n} = m_3 \qquad \text{on the body surface} \tag{12}$$

Here m_3 is given by

$$m_3 = - \left(n_2 \frac{\partial}{\partial y} + n_3 \frac{\partial}{\partial z} \right) \frac{\partial \phi_1}{\partial z} \tag{13}$$

There are two ways to solve for the potential ϕ_3: one is the multipole expansion method given by Ursell,[8] and the other is the close-fit method by Frank.[9] The solution of ϕ_3, using the former method, is given by

$$\phi_3 = \sigma_3 G_{2D}^{(0)} + \sum_{m=1}^{\infty} \alpha_m \left(\frac{\cos(2m\theta)}{r^{2m}} + \frac{K}{2m-1} \frac{\cos[(2m-1)\theta]}{r^{2m-1}} \right) \tag{14}$$

where σ_3 is the two-dimensional source strength located at the coordinate origin. The terms under the summation are the higher order multipoles which form the wave-free potentials with multipole strengths α_m. $G_{2D}^{(0)}$ is the two-dimensional Green function due to a source at the origin and is given by Wehausen and Laitone[10] as

$$G_{2D}^{(0)} = \frac{1}{\pi} PV \int_0^\infty \frac{e^{kz} \cos(ky)}{K-k} dk - i e^{Kz} \cos(Ky) \tag{15}$$

where $K = \omega^2/g$, and PV in Equation (15) denotes a principal value integral. The solution of ϕ_3 by the Frank close-fit method is

$$\phi_3 = \int_c \sigma G_{2D} \, d\ell \tag{16}$$

where σ is the source strength distributed on the ship's contour and G_{2D} is a two-dimensional Green function due to a unit source on the ship's contour. G_{2D}, in this case, is slightly different from Equation (15) and is given by

$$\begin{aligned} G_{2D} = \mathrm{Re}\left\{\frac{1}{2\pi}\left[\log(y+iz-\eta-i\zeta)-\log(y+iz-\eta+i\zeta)\right.\right. \\ \left.\left. + 2\ PV\int_0^\infty \frac{e^{-ik(y+iz-\eta+i\zeta)}}{K-k} dk\right]\right\} - i\ \mathrm{Re}(e^{-iK(y+iz-\eta+i\zeta)}) \\ + \mathrm{Re}\left\{\frac{1}{2\pi}\left[\log(y+iz+\eta-i\zeta)-\log(y+iz+\eta+i\zeta)\right.\right. \\ \left.\left. + 2\ PV\int_0^\infty \frac{e^{-ik(y+iz+\eta+i\zeta)}}{K-k} dk\right]\right\} - i\ \mathrm{Re}(e^{-iK(y+iz+\eta+i\zeta)}) \end{aligned} \tag{17}$$

Here (y,z) is the point where the potential is sought and (η,ζ) is a source point (Figure 2).

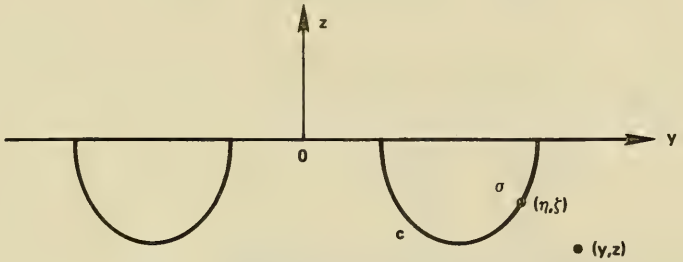

Figure 2 - Sectional Coordinate System

If (η,ζ) goes to the origin, the value of G_{2D} in Equation (17) becomes twice as large as that of Equation (15). By similar analogy, the solution of $\hat{\phi}_3$ is given by

$$\hat{\phi}_3 = \hat{\sigma}_3 \, G_{2D}^{(0)} + \sum_{m=1}^{\infty} \hat{\alpha}_m \left(\frac{\cos(2m\theta)}{r^{2m}} + \frac{K}{2m-1} \frac{\cos[(2m-1)\theta]}{r^{2m-1}} \right) \tag{18}$$

where $G_{2D}^{(0)}$ is given by Equation (15) and $\hat{\alpha}_m$ is the multipole strength. Both the σ_3 in Equation (14) and the σ in Equation (16) can be solved with application of the body boundary condition [Equation (9)]; $\hat{\sigma}_3$ in Equation (18) is solved using Equation (12).

The two-dimensional velocity potential due to pitch oscillation can be obtained by multiplying Equation (6) by -x to give

$$\varphi_5^{(S)} = - x(\phi_3 + \hat{\phi}_3) \tag{19}$$

TWO-DIMENSIONAL DIFFRACTION POTENTIAL

The two-dimensional diffraction potential satisfies the conditions

$$\frac{\partial^2 \varphi_7^{(S)}}{\partial y^2} + \frac{\partial^2 \varphi_7^{(S)}}{\partial z^2} = 0 \qquad \text{when } z < 0 \tag{20}$$

$$\frac{\partial \varphi_7^{(S)}}{\partial z} - \frac{\omega^2}{g} \varphi_7^{(S)} = 0 \qquad \text{on } z = 0 \tag{21}$$

and

$$\frac{\partial \varphi_7^{(S)}}{\partial n} = - \frac{\partial \varphi_o}{\partial n} \qquad \text{on the body surface} \tag{22}$$

Here φ_o is the potential of the incoming wave given by

$$\varphi_o = - \frac{igA}{\omega_o} \exp (K_o z + iK_o x \cos \beta - iK_o y \sin \beta) \tag{23}$$

where A = the amplitude of the incoming wave

β = the heading angle of the incoming wave ($\beta = 180°$ is for a head sea, and $\beta = 0°$ is for a following sea)

$K_o = \omega_o^2/g$

The solution of $\varphi_7^{(S)}$ satisfying Equations (20)-(22) is

$$\varphi_7^{(S)} = \int_c \sigma_d \, G_{2D} \, d\ell \tag{24}$$

where σ_d is the complex source strength at the ship's contour c, and G_{2D} is given by Equation (17).

UNIFIED SLENDER-BODY THEORY

The velocity potential due to oscillation is given by Newman[4] as

$$\varphi_j = \varphi_j^{(S)} + C_j(x) \, (\phi_j + \bar{\phi}_j) \quad (j=3,5) \tag{25}$$

where $\bar{\phi}_j$ is the conjugate of ϕ_j. The coefficient $C_j(x)$ is expressed by the integral

$$C_j(x) = \frac{i}{2\pi\bar{\sigma}_j} \int_L q_j(\xi)\, f(x-\xi)\, d\xi \tag{26}$$

where q_j is the three-dimensional source strength distributed along the 0x axis. This source strength is the solution of the following Fredholm integral equation of the second kind:

$$q_j(x) - i\left(\frac{\sigma_j+\bar{\sigma}_j}{2\pi\bar{\sigma}_j}\right)\int_L q_j(\xi)\, f(x-\xi)\, d\xi = \sigma_j + \hat{\sigma}_j \tag{27}$$

The kernel function f(x) is given by

$$f(x) = \ln(2K)\,\delta(x) + \frac{1}{2|x|} + \pi\, G_3(x) - i\pi\,\delta(x) \tag{28}$$

The Green function G_3 in this equation is

$$G_3(x,y,z;\xi,\eta,\zeta) = G(x,y,z;\xi,\eta,\zeta) - \frac{1}{r} - \frac{1}{r_1} \tag{29}$$

where

$$r = [(x-\xi)^2+(y-\eta)^2+(z-\zeta)^2]$$

and

$$r_1 = [(x-\xi)^2+(y-\eta)^2+(z+\zeta)^2]^{1/2}$$

and G is the three-dimensional Green function[10] given by

$$G(x,y,z;\xi,\eta,\zeta) = \frac{1}{r} - \frac{1}{r_1} + \frac{1}{\pi}\int_0^\infty du \int_{-\pi}^{\pi} \frac{u\, e^{(z+\zeta)u - i\,\overline{w}\,u}\, d\theta}{u-(\sqrt{m}\,u\cos\theta+\sqrt{K})^2} \tag{30}$$

Here, $\overline{w} = (x-\xi)\cos\theta + (y-\eta)\sin\theta$, and $m = u^2/g$.

By substituting Equation (30) into Equation (29), $G_3(x,0,0,0,0,0) \equiv G_3(x)$ is given by

$$G_3(x) = \frac{1}{2\pi}\int_{-\infty}^{\infty} du \int_0^{\pi} \frac{(\sqrt{K}+\sqrt{m}\,u\cos\theta)^2 \exp(-i\,x\,u\cos\theta)}{u - (\sqrt{K}+\sqrt{m}\,u\cos\theta)^2}\, d\theta \tag{31}$$

The diffraction potential of the unified slender-body theory is given by

$$\varphi_7 = \varphi_7^{(S)} + C_7(x)\ (\phi_s+\overline{\phi}_s) \tag{32}$$

where ϕ_s is the symmetric function of $\varphi_7^{(S)}$, $\overline{\phi}_s$ is the conjugate of ϕ_s, and $C_7(x)$ is

$$C_7(x) = -\frac{i}{2\pi\overline{\sigma}_7}\int_L q_7(\xi)\, f(x-\xi)\, d\xi \tag{33}$$

Here, q_7 is the solution of

$$q_7(x) - i\left(\frac{\sigma_7+\overline{\sigma}_7}{2\pi\overline{\sigma}_7}\right)\int_L q_7(\xi)\, f(x-\xi)\, d\xi = -\sigma_7 \tag{34}$$

ϕ_s in Equation (32) can be expressed as

$$\phi_s = G_{2D}^{(0)}\,\sigma_7 \tag{35}$$

where $G_{2D}^{(0)}$ is given by Equation (15). The two-dimensional source strength σ_d in Equation (24) is distributed on the ship's contour (Figure 2), and σ_7 is a concentrated source strength at the origin. In other words, σ_d is the solution of the Frank close-fit method and σ_7 is the solution of the multipole expansion method. The relation between σ_d and σ_7 can be expressed by

$$\sigma_7 = 2 \int_c \sigma_d \, e^{K\zeta} \cos K\eta \, d\ell \tag{36}$$

The same relation between σ_3 and σ is given by

$$\sigma_3 = 2 \int_c \sigma \, e^{K\zeta} \cos K\eta \, d\ell \tag{37}$$

The total unsteady potential ϕ_2 for heave and pitch motion is given by Equations (23), (25), and (32):

$$\phi_2 = \varphi_0 + \varphi_7 + \xi_3 \varphi_3 + \xi_5 \varphi_5 \tag{38}$$

where ξ_3 is the heave amplitude and ξ_5 is the pitch amplitude. In the frame of the unified slender-body theory, only heave and pitch motions are considered. The pressure p in the fluid is given by Bernoulli's equation

$$p = \rho(i\omega\phi_2 - \nabla\phi_1 \cdot \nabla\phi_2) \, e^{-i\omega t} - \rho g \zeta \tag{39}$$

By substituting Equation (38) into Equation (39) and integrating on the body surface, the hydrodynamic forces are expressed by

$$f_j = -\rho \iint_S (i\omega n_j + m_j)(\varphi_0 + \varphi_7 + \xi_3\varphi_3 + \xi_5\varphi_5) \, dS \, e^{-i\omega t} \quad (j=3,5) \tag{40}$$

where n_5 and m_5 are given by

$$n_5 = -xn_3 \tag{41}$$

and

$$m_5 = -xm_3 + n_3 \tag{42}$$

The first two potential terms in parentheses in Equation (40) represent the exciting forces, and the other two potential terms are due to the added-mass and damping forces. Complete lists of added-mass and damping forces are given in Table 1 of Reference 6. Further, the detailed derivations of all equations not derived in this report are given in References 4 and 6.

SINGULARITY OF THE KERNEL FUNCTION

The procedure employed here to compute the hydrodynamic forces and the motion begins by solving for σ_3 and $\hat{\sigma}_3$ in Equations (14) and (18) through the use of strip theory. The kernel function $f(x)$ of Equation (28) is computed and retained for later use. Next, the three-dimensional source strength $q_j(x)$ is computed by solving the Fredholm Integral Equation (27). Once $q_j(x)$ is obtained, the sectional interaction coefficient $C_j(x)$ may be computed through Equation (26).

The most difficult and time-consuming part of numerical computation is the evaluation of the kernel function Equation (28) and the three-dimensional source strength Equation (27). In a previous publication[6] the present author presented a numerical method for the evaluation of the kernel function, Equation (28), through a small-order procedure in order to avoid the $1/|x|$-type singularity. However, this method is not generally applicable to the SWATH ship motion problem since the solution is not uniform, i.e., the predicted response depends upon the size of the small-order parameter. In order to avoid this singularity, Equation (27) may be integrated by parts to yield

$$q_j(x) - i\left(\frac{\sigma_j+\bar{\sigma}_j}{2\pi\bar{\sigma}_j}\right)\left\{-q_j(\xi)F(x-\xi)\Big|_{-L/2}^{L/2} + \int_L q_j'(\xi)F(x-\xi)d\xi\right\} = \sigma_j + \hat{\sigma}_j \qquad (j=3,5) \tag{43}$$

where $q_j'(x)$ is the derivative of $q_j(x)$ with respect to x; the function $F(x)$ is the integral of Equation (28) with respect to x:

$$F(x) = \frac{1}{2} \text{ Sgn } x(\ell n(2K|x|)-i\pi+\gamma) + \pi \int_0^x G_3(\xi)\, d\xi \tag{44}$$

Here, Sgn x is defined as 1 when $x < 0$, -1 when $x > 0$, and undefined at $x = 0$, and γ, Euler's constant, is 0.57721.... The integrated term in Equation (43) can be expressed as

$$\lim_{\varepsilon \to 0} \left\{ -q_j(\xi)F(x-\xi)\Big|_{\xi=-L/2}^{\xi=x-\varepsilon} - q_j(\xi)F(x-\xi)\Big|_{\xi=x+\varepsilon}^{\xi=L/2} \right\} \tag{45}$$

Since $q_j(-L/2)$ and $q_j(L/2)$ are assumed to be zero, Equation (45) is further reduced to

$$\lim_{\varepsilon \to 0} \{-q_j(x-\varepsilon)F(\varepsilon)+q_j(x+\varepsilon)F(-\varepsilon)\} \tag{46}$$

As $q_j(x)$ is a continuous function along the ship's length, Equation (46) can be written as

$$- \lim_{\varepsilon \to 0} \{q_j(x)[F(\varepsilon)-F(-\varepsilon)]\} \tag{47}$$

$F(\varepsilon)$ has a singularity as $\varepsilon \to 0$. This singularity occurs because of the limits of the integral and can be omitted with the interpretation that the "finite part" defined by Hadamard obeys many of the ordinary rules of integration.[11,12] By discarding the integrated term, the integral equation for $q_j(x)$ becomes

$$q_j(x) - i\left(\frac{\sigma_j+\bar{\sigma}_j}{2\pi\bar{\sigma}_j}\right)\int_L q'(\xi)\, F(x-\xi)\, d\xi = \sigma_j + \hat{\sigma}_j \qquad (j=3,5) \tag{48}$$

The numerical solution of Equation (48) is accomplished by iterating. One disadvantage of this method is that the numerical method does not converge when the

forward speed is high. To overcome this convergence problem, it is instructive to compare Equations (27) and (48). Equation (27) can be solved by the matrix inversion or Gauss-Jordan method as long as the singularity problem in f(x) is solved. By defining a new function,

$$h(x-\xi) = f(x-\xi) \qquad \xi \neq x \tag{49}$$

and

$$h(x-\xi) = f(x-\xi) + [F(\varepsilon)-F(-\varepsilon)] \qquad \xi = x$$

the integral equation

$$q_j(x) - i\left(\frac{\sigma_j+\bar{\sigma}_j}{2\pi\bar{\sigma}_j}\right)\int_L q_j(\xi)\, h(x-\xi)\, d\xi = \sigma_j + \hat{\sigma}_j \qquad (j=3,5) \tag{50}$$

has the same solution as Equation (48). The advantage of solving Equation (50) is that the matrix inversion method can be applied to it and has been found to yield solutions for all speed ranges. In the low-speed range, the iteration method works satisfactorily and, in this case, the solution of Equation (50) compares well with that of Equation (48).

RESULTS AND DISCUSSION

In order to validate the numerical results of the present unified slender-body theory, three hull forms have been selected: a twin ellipsoid hull, the SWATH 6A hull, and the SWATH 6D hull form. The principal parameter values for these three hull forms are given in Table 1. The twin ellipsoid is a mathematically exact hull, and its performance at zero speed may be compared with the predictions of the strip theory and the three-dimensional theory. The computations for SWATH 6A and SWATH 6D have been carried out for speeds of 28 knots in head seas and 20 knots in following seas. These results are compared with those of strip theory and experiments.

Numerical computations for the twin ellipsoid have been carried out at zero speed in head seas and are shown in Figures 3-6. In this case the three-dimensional

TABLE 1 - VALUES OF PRINCIPAL PARAMETERS FOR THREE HULL MODELS*

Parameter (and Unit)	Hull Form		
	SWATH 6A	SWATH 6D	Twin Ellipsoid
Displacement (long ton)	2579	2815	1.823
Characteristic length L (m)	54.3	73.1	6.1
Length of waterline (m)	52.5	68.0	6.096
Length of main hull (m)	73.2	73.2	6.096
Beam of each hull at waterline (m)	2.2	2.2	0.762
Hull spacing between centerline (m)	22.9	22.9	1.143
Draft at midship (m)	8.1	8.1	0.381
Maximum diameter of main hull (m)	4.6	4.6	--
Longitudinal center of gravity aft of main hull nose (m)	35.5	36.1	3.048
Vertical center of gravity (m)	10.4	9.1	0.381
Longitudinal GM (m)	6.1	26.4	6.096
Radius of gyration for pitch (m)	16.9	19.0	1.2192
Waterplane area (m)	193.9	211.2	7.297
Length of strut (m)	52.4	25.8/strut	--
Strut gap (m)	0.0	16.4	--
Maximum strut thickness (m)	2.2	3.1	--

*Dimensions are full-scale.

theory is exact. The added-mass coefficients A_{ii}, i = 3, 5, computed with the slender-body theory compare better with the three-dimensional results than with those of the strip theory. This is especially true at low frequencies. At high frequencies the results of the strip theory and the slender-body theory are almost the same, as in Reference 4 in which the kernel functions of Equation (27) vanish. The abrupt changes in the curves of added-mass and damping coefficients are due to the hydrodynamic interaction of the two hulls when the (nondimensional) frequency is approximately 2.5.

The exciting forces F_3 and moments F_5 are shown in Figure 5. The slender-body theory predictions for pitch moments F_5 are found to be nearly the same as those of the strip theory, but higher than those of the three-dimensional theory. The

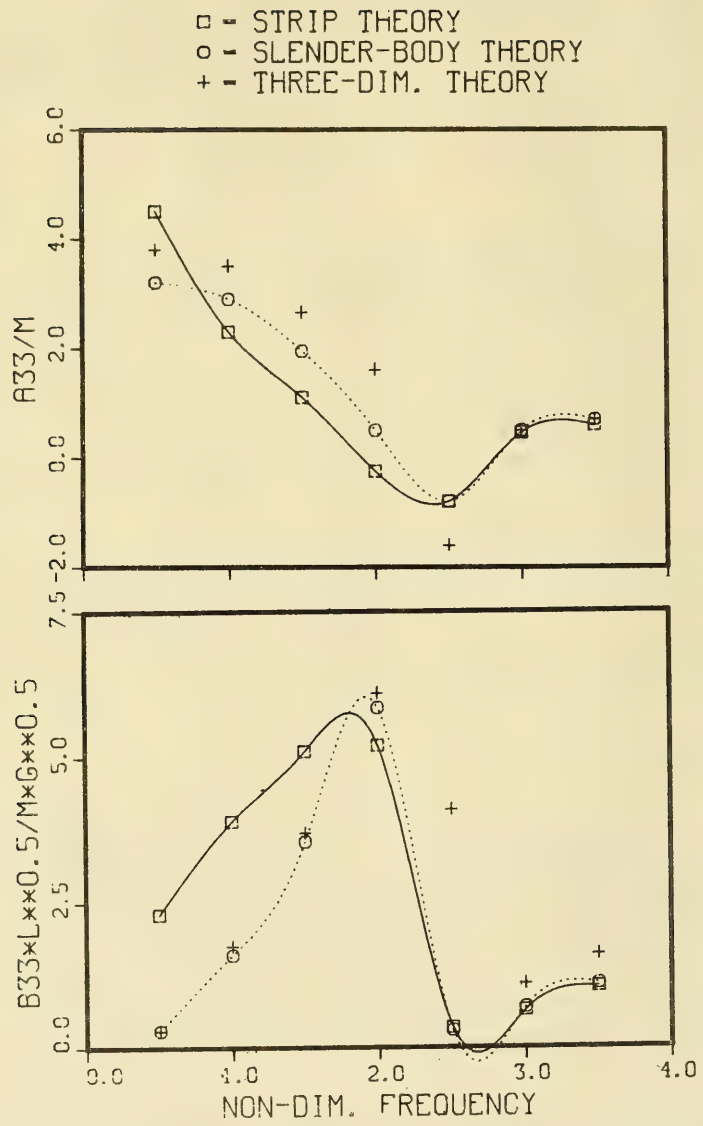

Figure 3 - Heave Added-Mass and Damping Coefficients of Twin Ellipsoid in Head Seas at Zero Speed

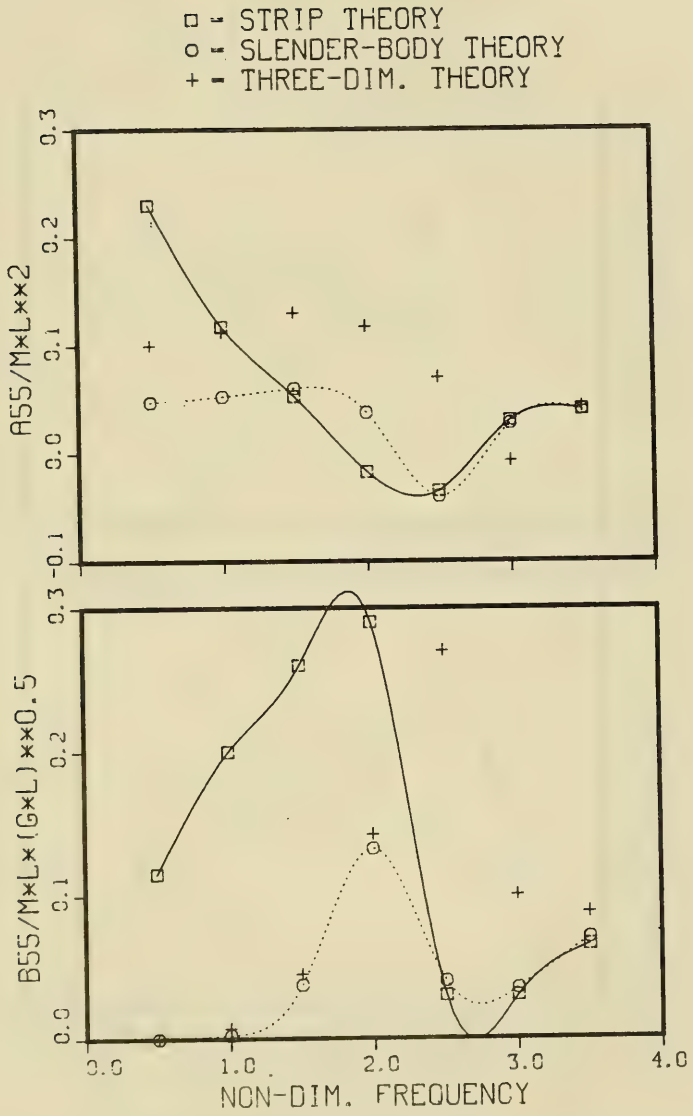

Figure 4 - Pitch Added-Mass and Damping Coefficients of Twin Ellipsoid in Head Seas at Zero Speed

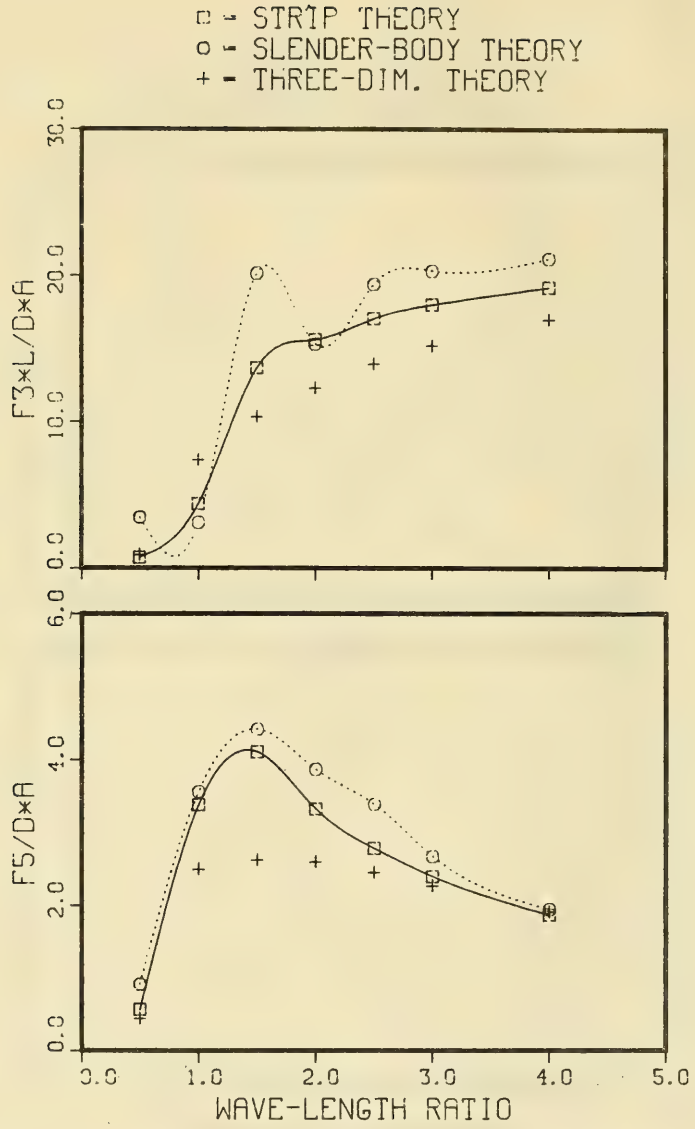

Figure 5 - Heave Exciting Forces and Pitch Exciting Moments of Twin Ellipsoid in Head Seas at Zero Speed

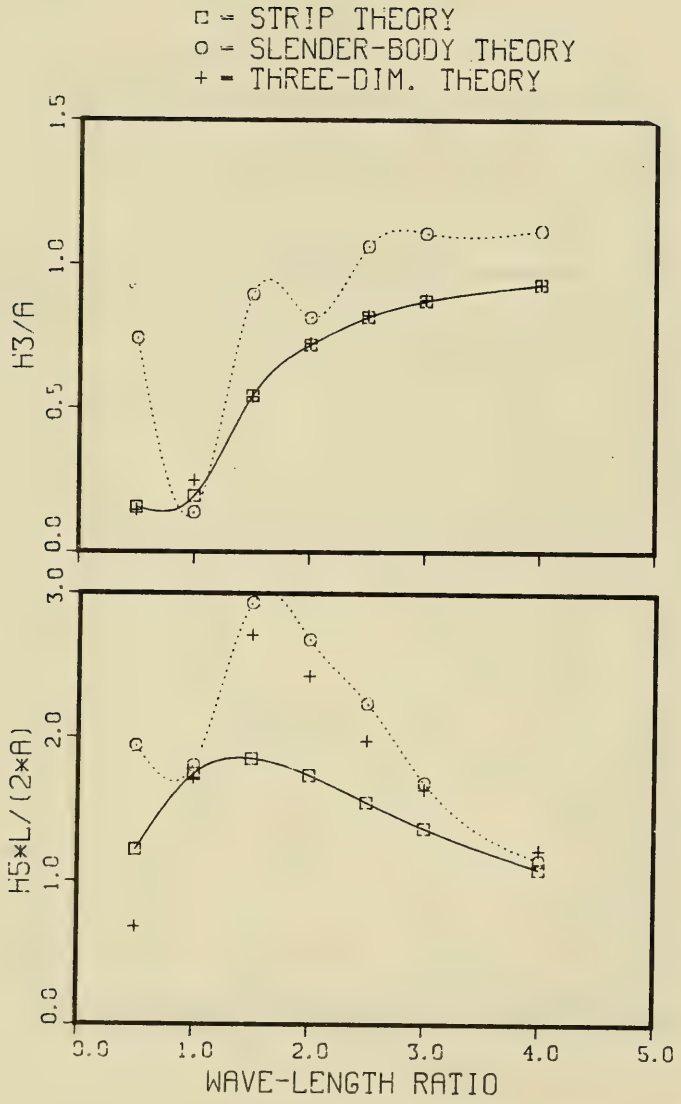

Figure 6 - Heave and Pitch Amplitudes of Twin Ellipsoid in Head Seas at Zero Speed

slender-body heave amplitudes shown in Figure 6 are greater than those of both the strip theory and the three-dimensional theory. The pitch amplitudes agree quite well even though the pitch moments are computed differently. For the twin ellipsoidal hulls, the damping coefficients are almost the same, the added-mass coefficients are computed as slightly less, and the exciting moments are higher than those predicted by the three-dimensional theory. In the case of pitch amplitude, it appears that the underprediction of the added-mass coefficients and the overprediction for the exciting forces cancel out in the motion results.

In a previous report[6] this author presented an explanation for the rather large discrepancies in the added-mass coefficients computed through Equation (37) employing the singularity distribution σ_3. Since that publication, the author has computed the singularity distribution σ_3 directly through the multipole expansion method for the semicircular section and has compared this result with Equation (37); the two computations agree quite well. Unfortunately, for the twin-hull section, the direct computation σ_3 through Equation (14) is apparently impossible. Therefore, σ_3 has been computed for all models through Equation (37). The large discrepancies mentioned above have been identified as the result of a different numerical handling of the singularities of the kernel function. As shown later, the prediction of the added-mass coefficients in following seas has the same tendency--lower at low frequencies and higher at high frequencies than those of the strip theory.

The results for SWATH 6A at 28 knots in head seas are shown in Figures 7-10. The added-mass and damping coefficients do not show any difference when compared with those of the strip theory. While our interest range is in wavelength ratios between 1 and 6, the corresponding nondimensional frequency number varies from 2 to 6. These frequency numbers are fairly high, and, therefore, the slender-body theory does not improve the prediction of the added-mass and damping coefficients. However, the exciting forces and moments show large discrepancies when compared with those computed through theory. This is due to the fact that whereas the two-dimensional source strength σ_7 for the diffraction potential has the factor $\exp(iK_0 x \cos \beta)$ in Equation (23), σ_7 in Equation (36) varies harmonically along the ship's length. This sinusoidal change of σ_7 affects the solution of q_7 in Equation (34) and also the solution change of C_7 in Equation (33). The oscillatory behavior of the exciting forces and moments is caused by this solution for C_7. The heave and pitch amplitudes show some discrepancies between experiment and the strip theory. The mixed

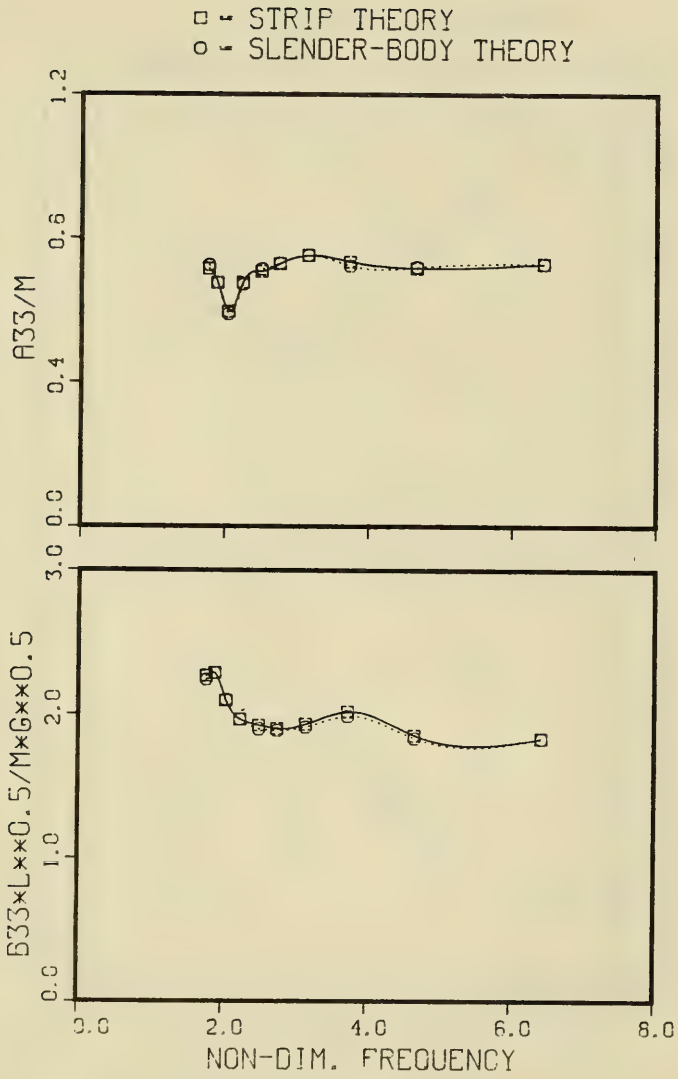

Figure 7 - Heave Added-Mass and Damping Coefficients of SWATH 6A in Head Seas at 28 Knots

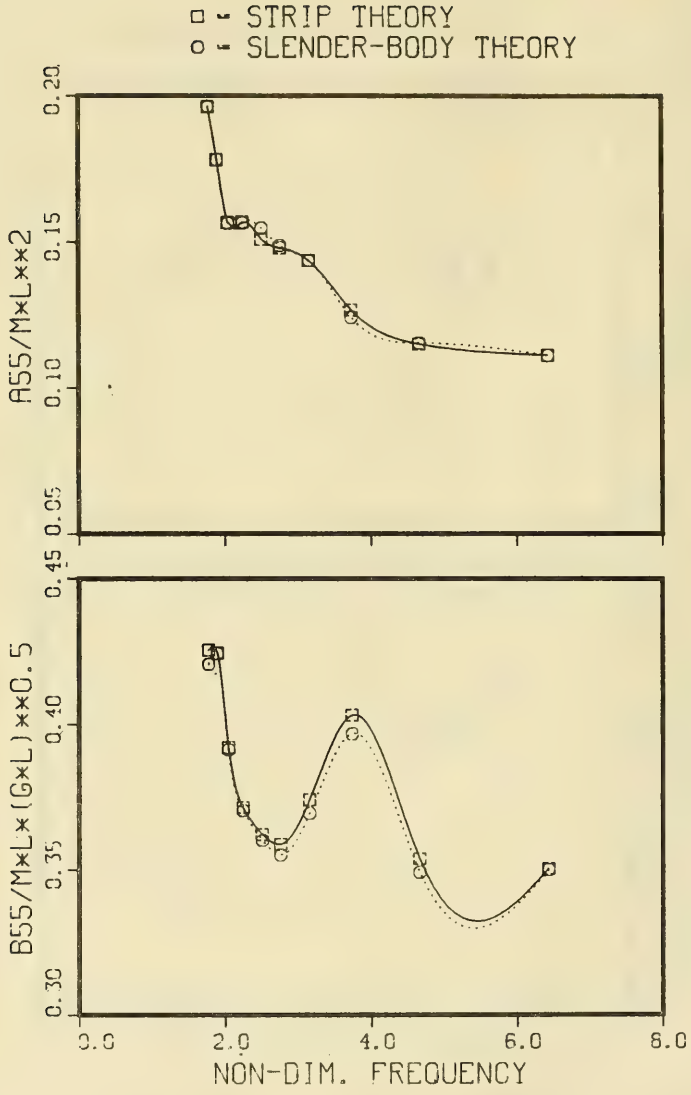

Figure 8 - Pitch Added-Mass and Damping Coefficients of SWATH 6A in Head Seas at 28 Knots

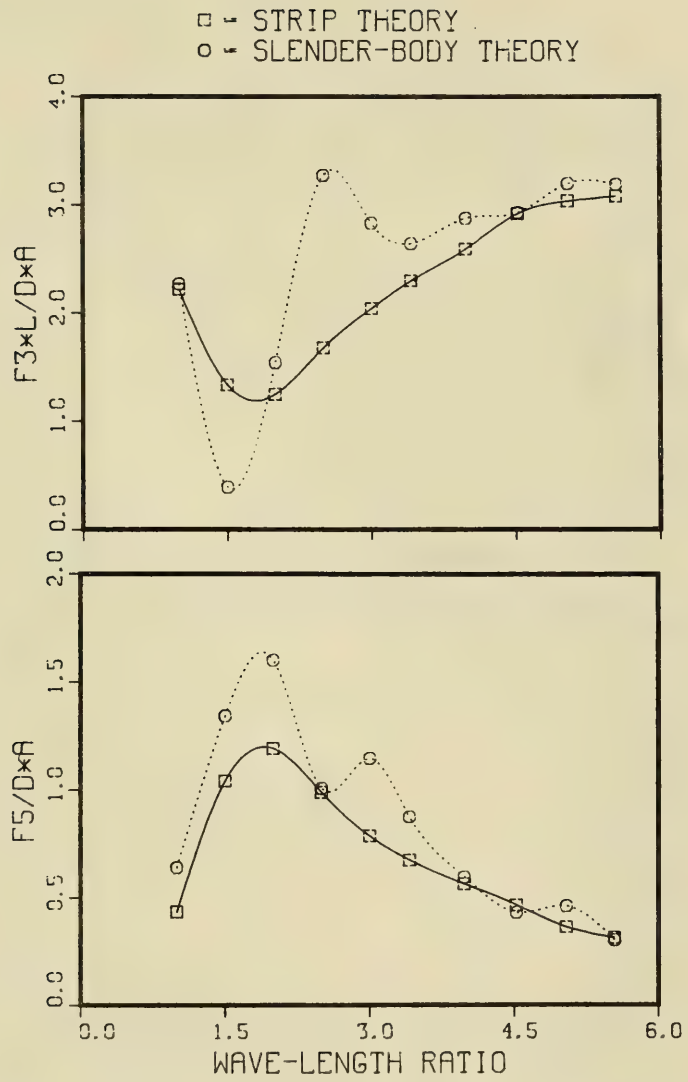

Figure 9 - Heave Exciting Forces and Pitch Exciting Moments of SWATH 6A in Head Seas at 28 Knots

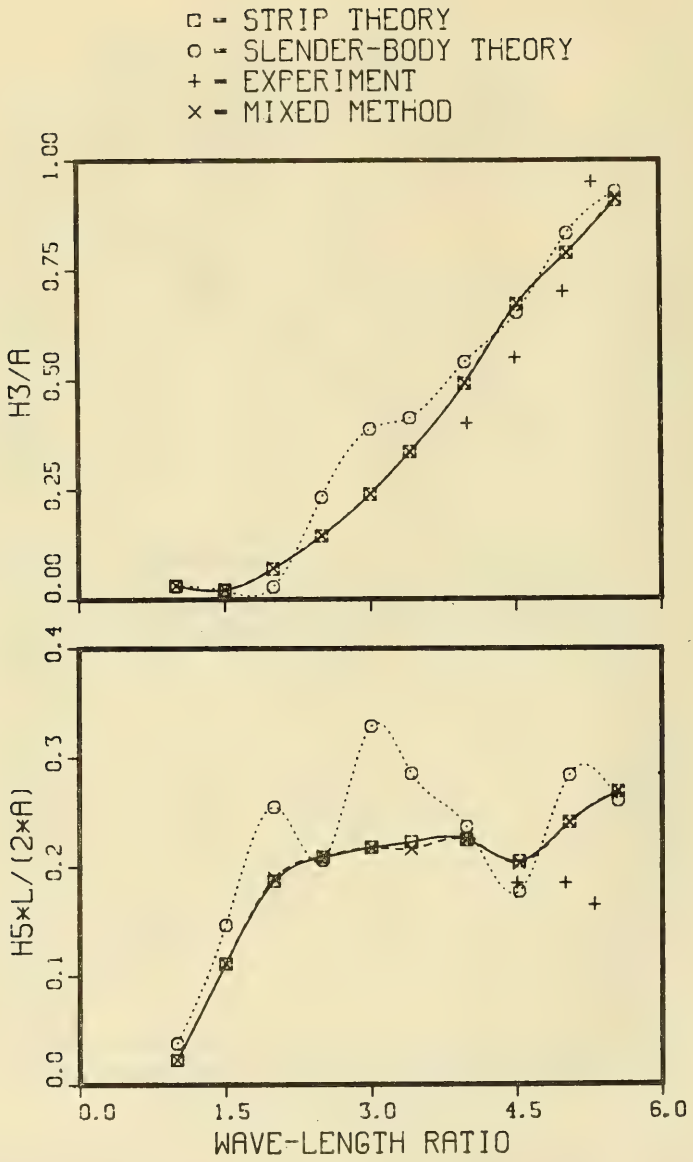

Figure 10 - Heave and Pitch Amplitudes of SWATH 6A in Head Seas at 28 Knots

method is the result of the combination of the strip theory and slender-body theory. In the mixed method the added-mass and damping coefficients are computed through slender-body theory, while the exciting forces and moments are computed through the strip theory. The results obtained with the mixed method are generally the same as those of the strip theory. This means that the effect on motion amplitude of the added-mass and damping coefficients computed with the slender-body theory is negligible in this example and that the oscillatory results in the pitch motion are caused by the pitch moments.

The results of SWATH 6D at 28 knots in head seas are shown in Figures 11-14. As previously noted for the SWATH 6A, the added-mass and damping coefficients of the slender-body theory do not show any difference from those of the strip theory, except in the low-frequency range where the slender-body theory values for the hydrodynamic coefficients are lower than those of the strip theory. In the (nondimensional) frequency range between 1.5 and 4.0, the slender-body heave forces F_3 show the same tendency as those of the strip theory, and the pitch moments F_5 display oscillatory behavior at low wavelength ratios (Figure 13). This phenomenon is also observed in the results of the SWATH 6A.

In the previous report,[6] the results for SWATH 6A and 6D at 20 knots in following seas have been compared with those of the strip theory and experiment. Since the numerical procedure has been corrected in the computation of the kernel function, the computations of the following seas have been repeated in this report. These results for SWATH 6A are plotted in Figures 15-18. When the nondimensionalized frequency is 0.56, there exists a discontinuity in the curves of the hydrodynamic coefficients. As mentioned in the previous report,[6] when $\omega U/g$ is 0.25, G_3 of Equation (31) is singular and the numerical results become unstable. The damping coefficients are nearly the same as those obtained through strip theory, except where this discontinuity occurs. Compared with the previous results, the damping coefficients do not show any change; however, the added-mass coefficients are quite different. While the previous results are uniformly greater than those of the strip theory, the present ones are less at low frequency and greater at high frequency. The results of the exciting forces and moments computed by the slender-body theory and by the strip theory are similar, except there is a peak value in the pitch moment computed by the slender-body theory for a wavelength ratio of approximately 2.0. The motion results are also similar to those computed by strip theory, except at the peak value for a wavelength ratio of approximately 1.5. When the wavelength ratio is 1.3, the

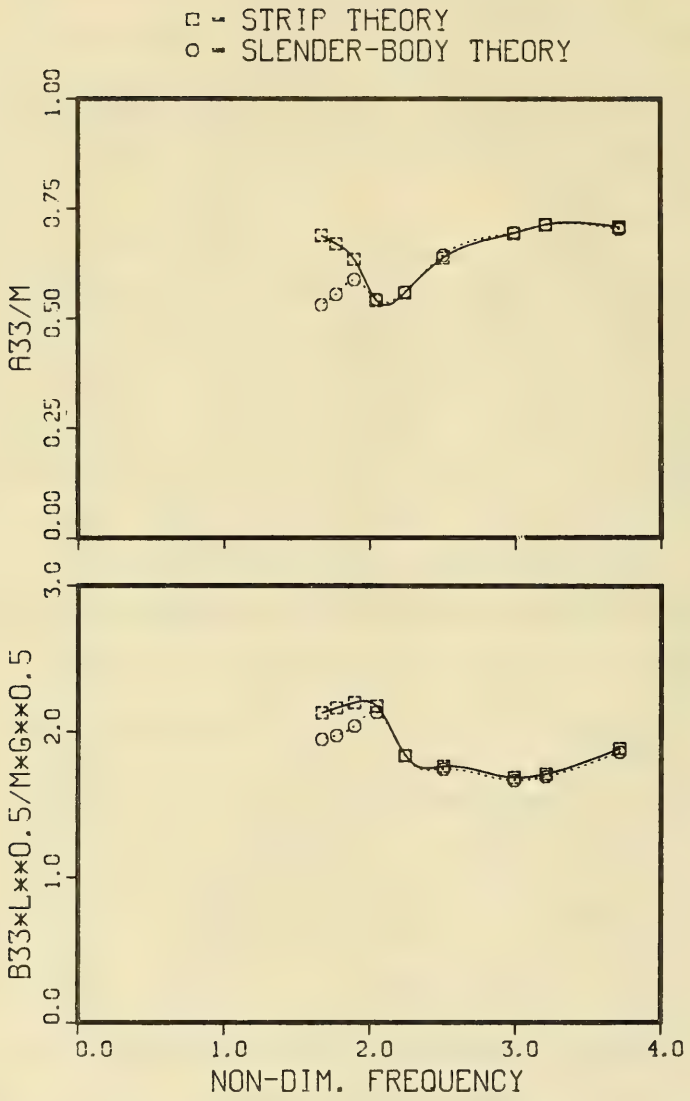

Figure 11 - Heave Added-Mass and Damping Coefficients of SWATH 6D in Head Seas at 28 Knots

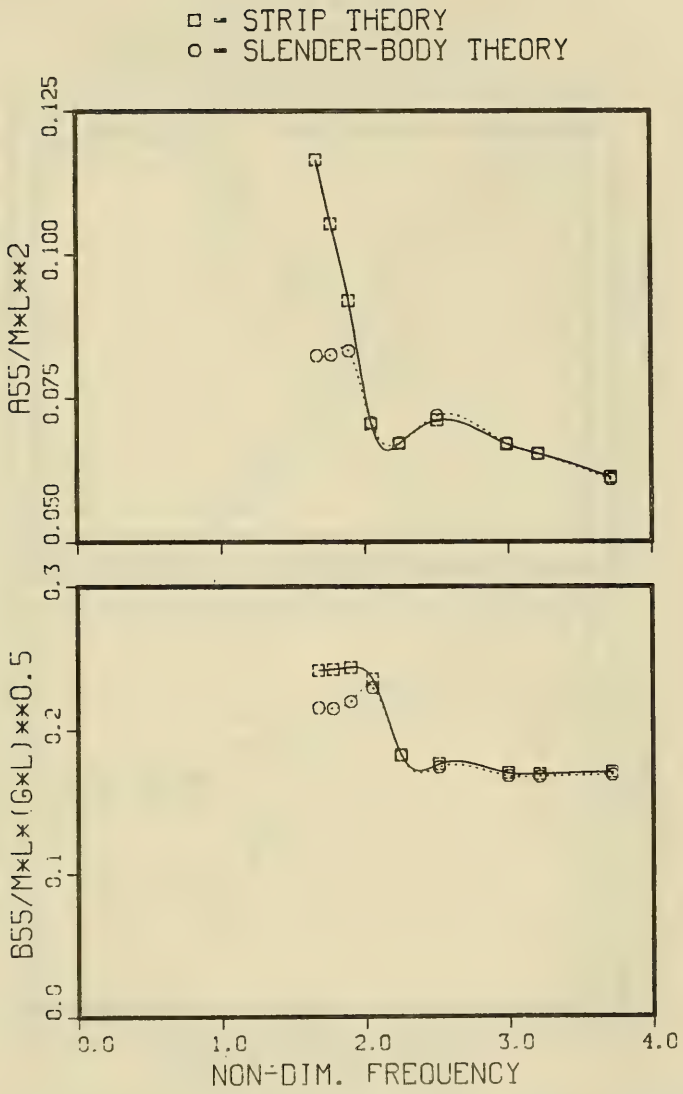

Figure 12 - Pitch Added-Mass and Damping Coefficients of SWATH 6D in Head Seas at 28 Knots

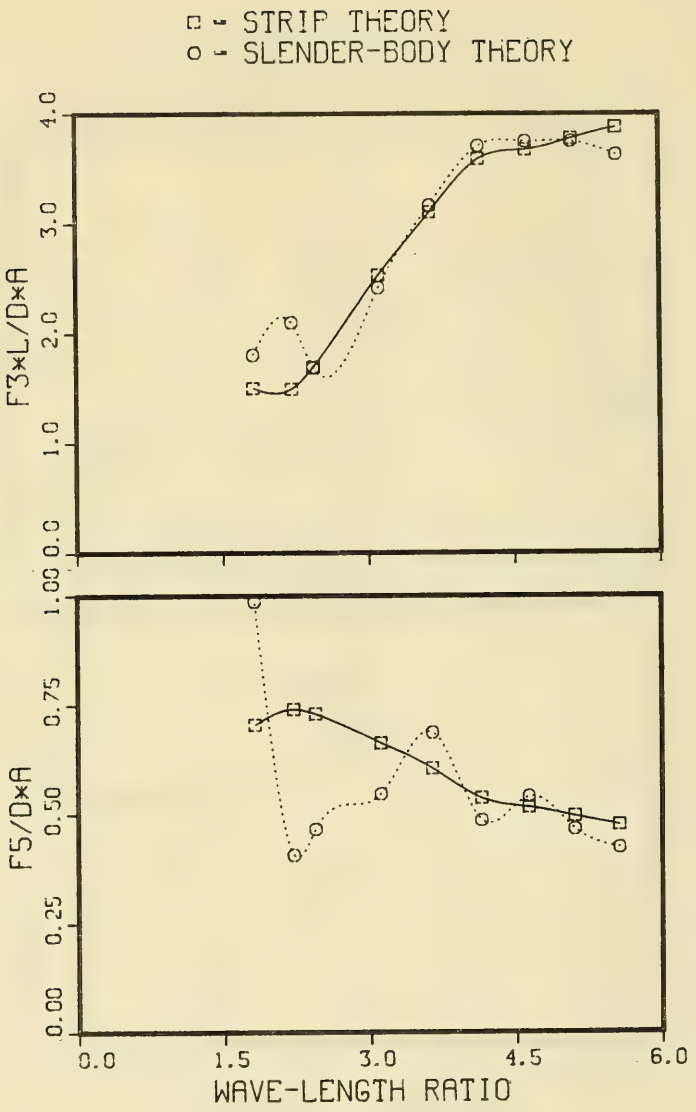

Figure 13 - Heave Exciting Forces and Pitch Exciting Moments of SWATH 6D in Head Seas at 28 Knots

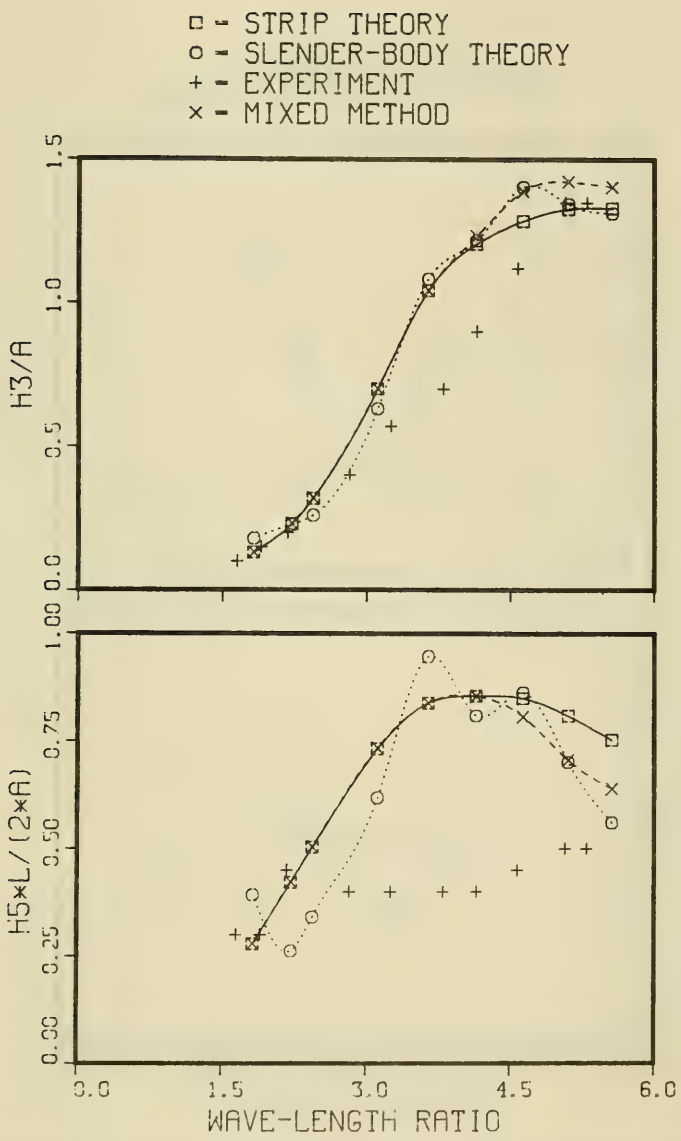

Figure 14 - Heave and Pitch Amplitudes of SWATH 6D in Head Seas at 28 Knots

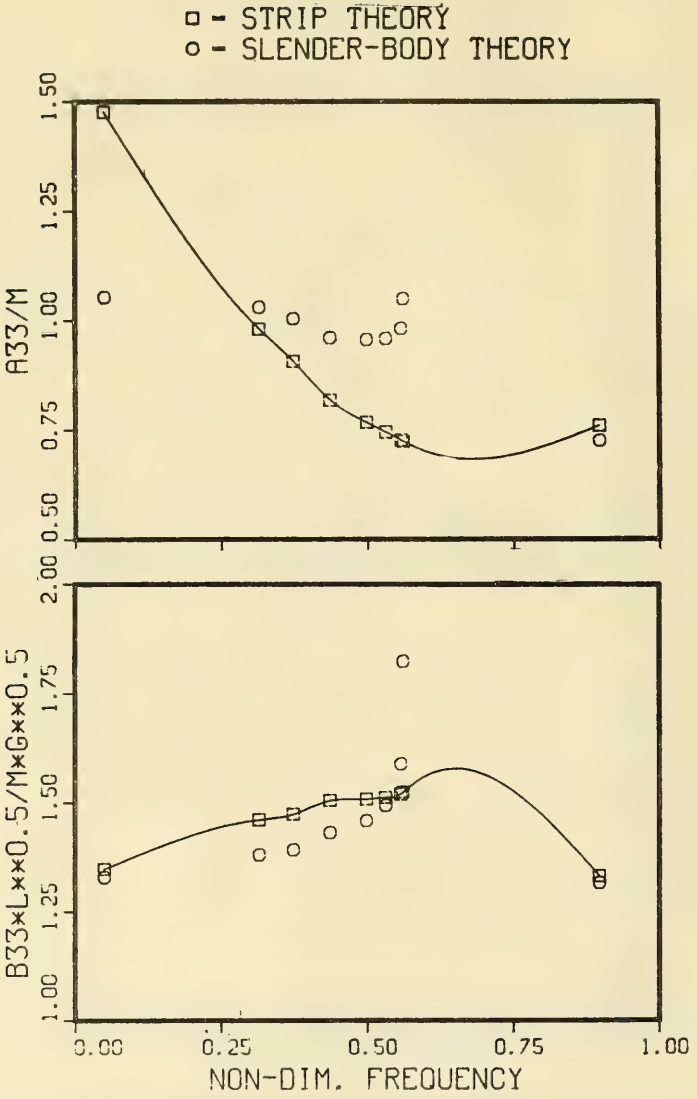

Figure 15 - Heave Added-Mass and Damping Coefficients of SWATH 6A in Following Seas at 20 Knots

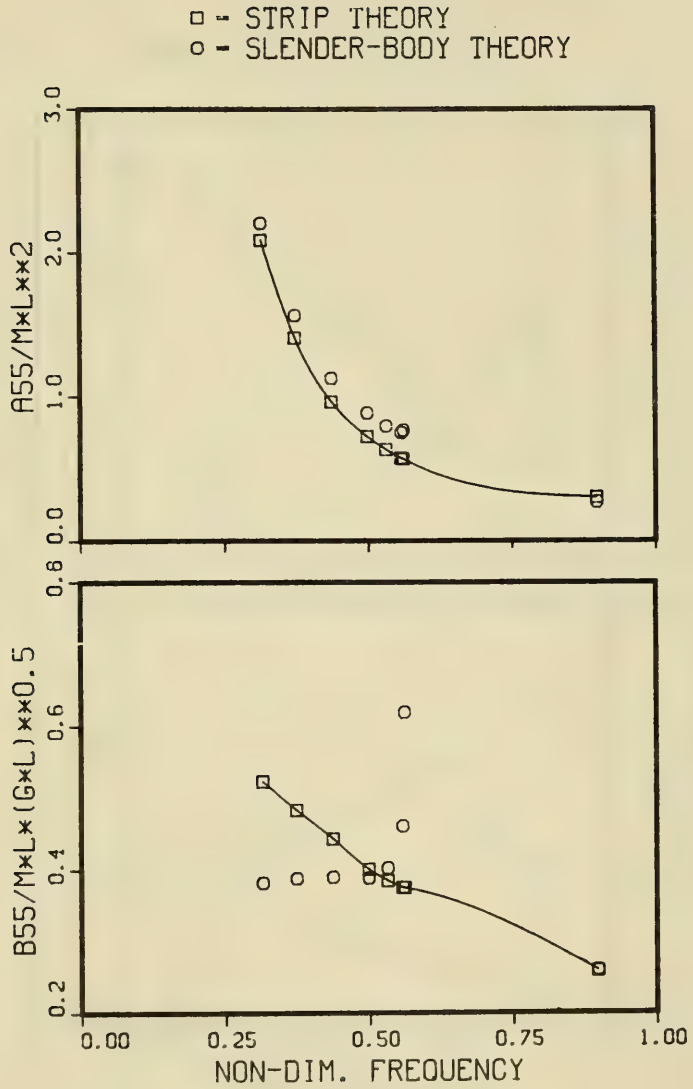

Figure 16 - Pitch Added-Mass and Damping Coefficients of SWATH 6A in Following Seas at 20 Knots

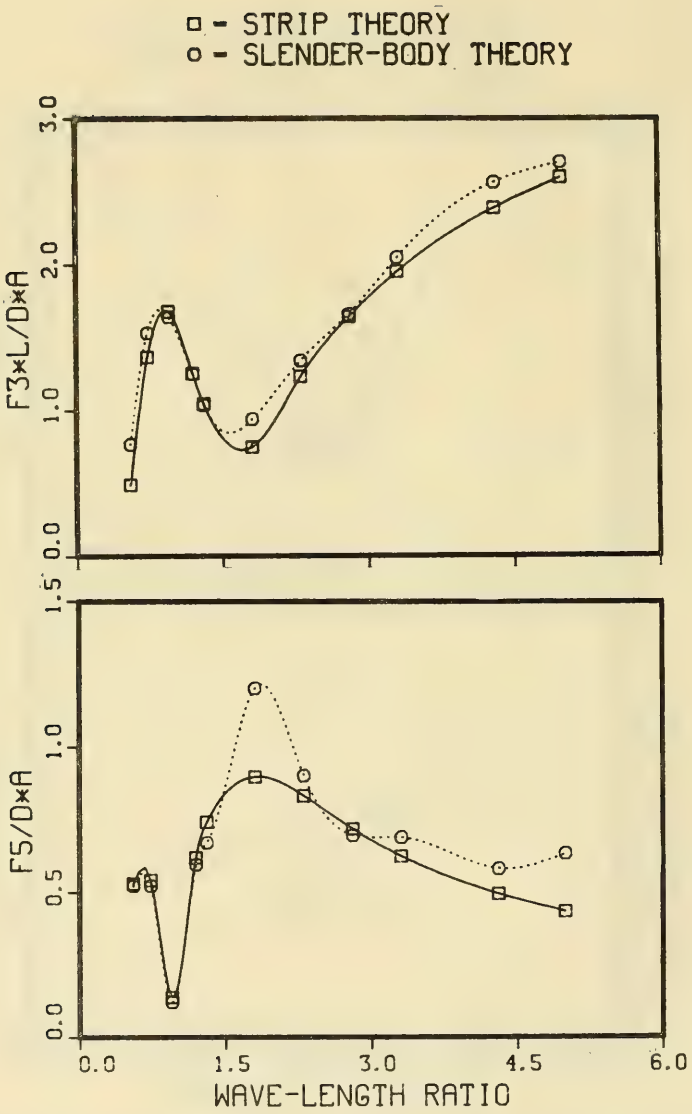

Figure 17 - Heave Exciting Forces and Pitch Exciting Moments of SWATH 6A in Following Seas at 20 Knots

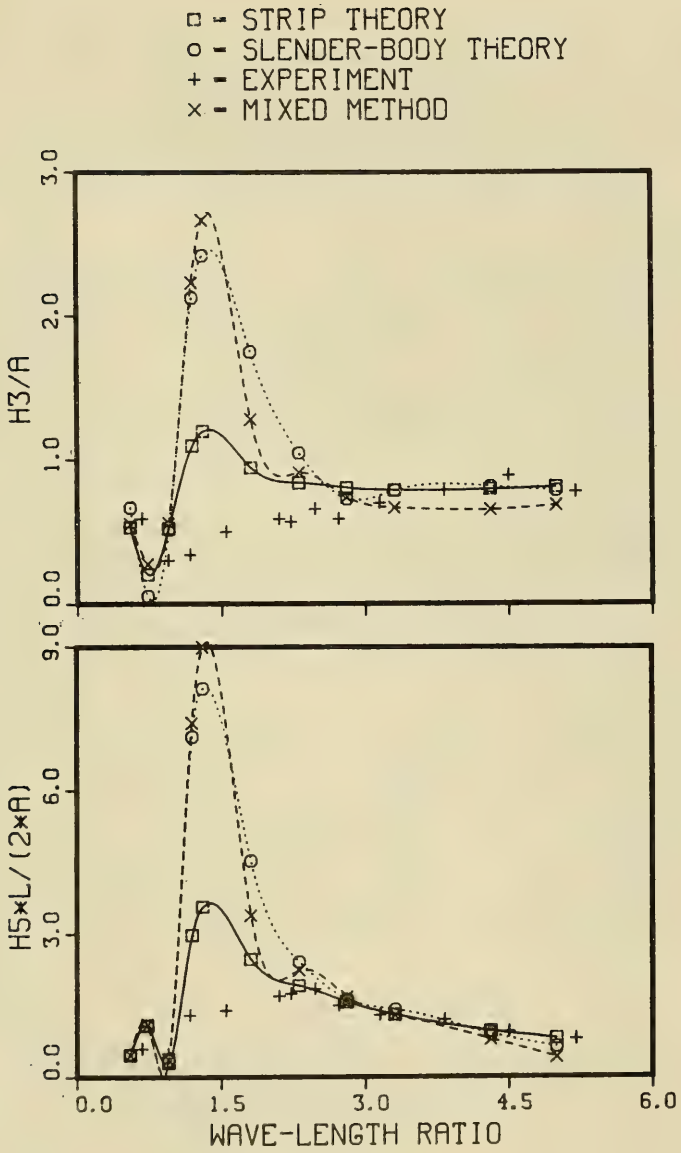

Figure 18 - Heave and Pitch Amplitudes of SWATH 6A in Following Seas at 20 Knots

nondimensionalized frequency number becomes zero and the computed hydrodynamic coefficients are far smaller than those predicted by strip theory. Therefore, the motion amplitudes are magnified at this wavelength ratio. If we compare the results of the strip theory and the mixed method, this magnification effect is easily seen in the motion results. In the mixed method, the hydrodynamic coefficients are computed by the slender-body theory, and the exciting forces and moments are computed by strip theory.

The results for SWATH 6D at 20 knots in following seas are plotted in Figures 19-22. When the nondimensionalized frequency number is 0.65 ($\omega U/g=0.25$), there is a discontinuity in the curve of the hydrodynamic coefficients similar to that observed in the calculations for SWATH 6A. These coefficients are found to be smaller at low frequencies and larger at high frequencies than those computed through strip theory. While the heave exciting forces are overpredicted when compared with those of the strip theory and the experiments, the pitch moments are underpredicted for both results. All computed heave motions are in close agreement at low wavelength ratios, but for high wavelength ratios, discrepancies between experiment and computations are quite large. Pitch motions are in good agreement with the experimental results, except near a wavelength ratio of 1.0 where the encounter frequency becomes zero. The pitch moments computed by the strip theory are less than those obtained experimentally, but the pitch motions are larger. Generally, the motion results are affected by the inertia, hydrodynamic, and hydrostatic forces. Therefore, it is very difficult to determine the exact cause of these discrepancies.

Although there is a peak response shown in the motion of SWATH 6A in Figure 18, SWATH 6D (Figure 22) does not show such a peak value. This difference can be analyzed through the motion equations. If the coupling effect between heave and pitch motion is neglected, the solution of the pitch motion becomes

$$\xi_R = \{F_R[C_{55}-(I+A_{55})\omega^2]-F_I\omega B_{55}\}/\overline{D}$$

$$\xi_I = \{F_I[C_{55}-(I+A_{55})\omega^2]+F_R\omega B_{55}\}/\overline{D}$$

where

$$\overline{D} = [C_{55}-(I+A_{55})\omega^2]^2 + (\omega B_{55})^2$$

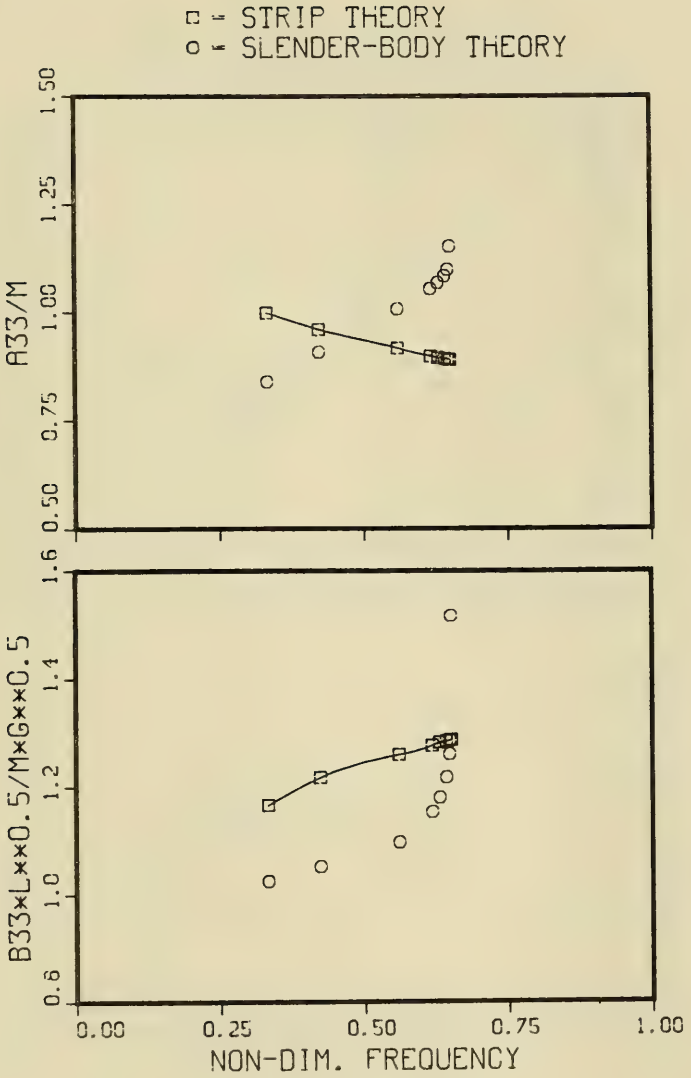

Figure 19 - Heave Added-Mass and Damping Coefficients of SWATH 6D in Following Seas at 20 Knots

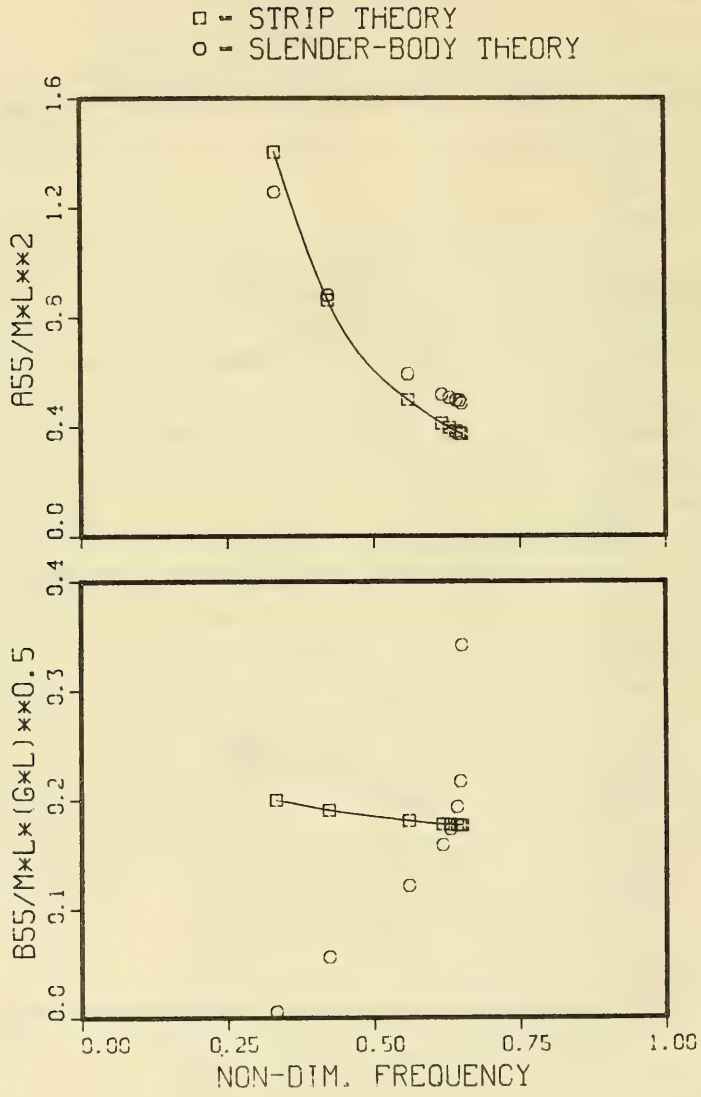

Figure 20 - Pitch Added-Mass and Damping Coefficients of SWATH 6D in Following Seas at 20 Knots

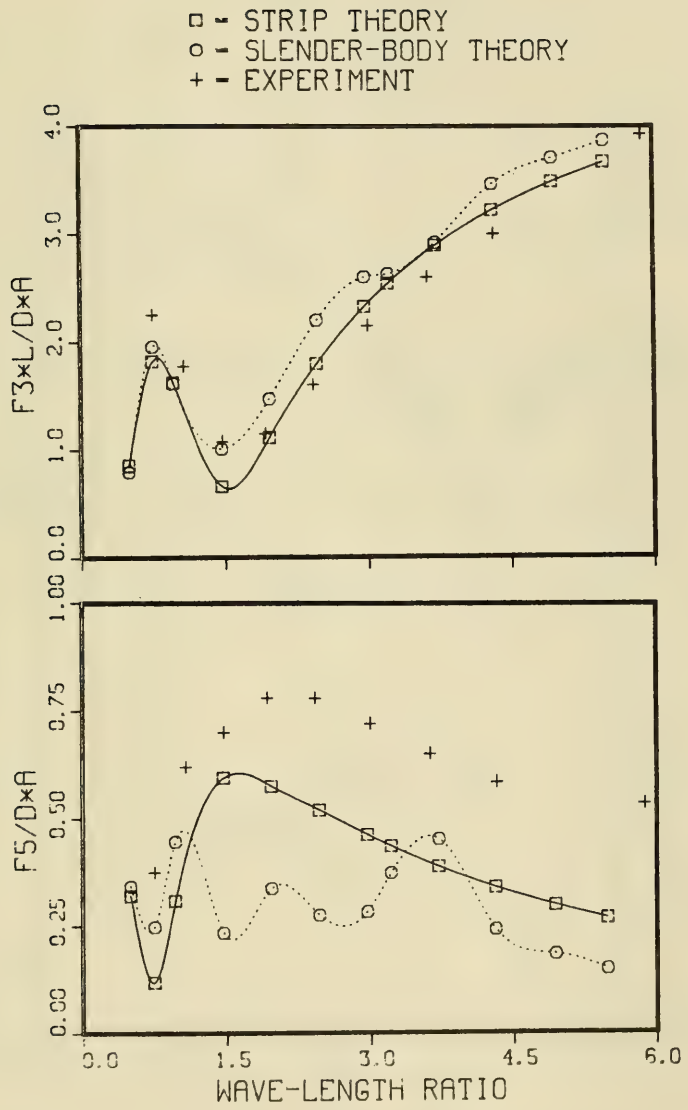

Figure 21 - Heave Exciting Forces and Pitch Exciting Moments of SWATH 6D in Following Seas at 20 Knots

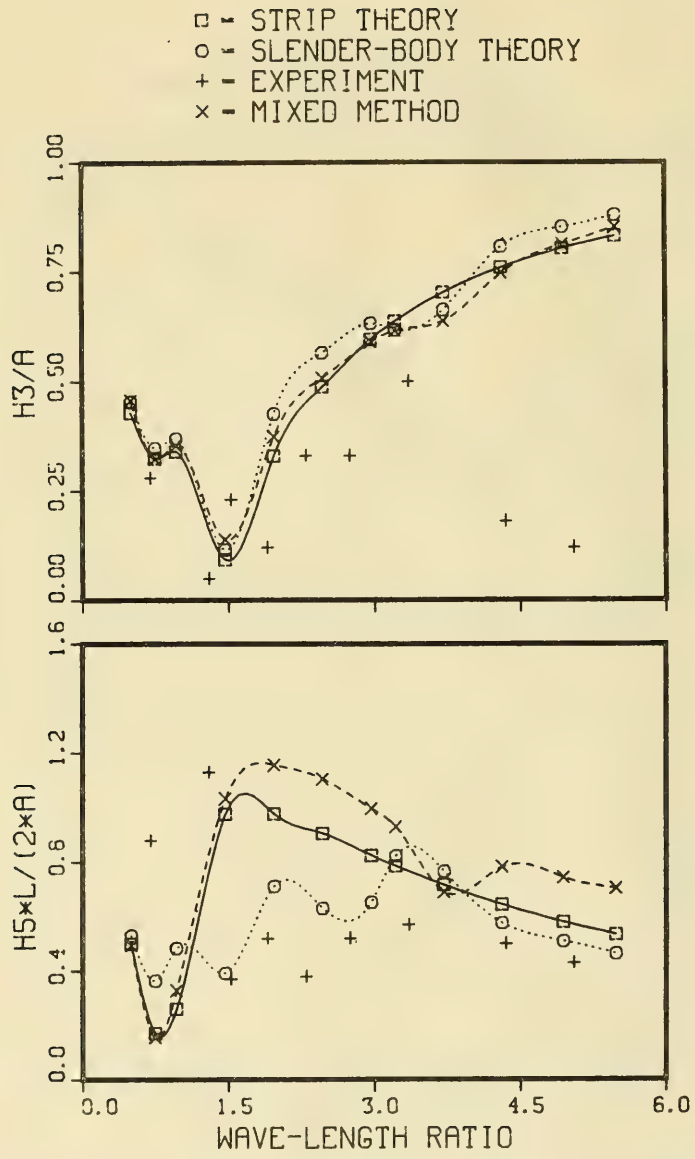

Figure 22 - Heave and Pitch Amplitudes of SWATH 6D in Following Seas at 20 Knots

The subscript R defines the real part and I the imaginary part of the complex functions. The peak value of SWATH 6A occurs near the point where the frequency becomes zero. Near zero, the pitch exciting moments for both SWATH ships are almost the same for both the strip theory and the slender-body theory. In this case, the major factors which determine the pitch amplitudes are C_{55}, A_{55}, and B_{55}. The peak value occurs when the pitch determinant $\overline{D}$ becomes small. Numerical values for these coefficients are presented in Table 2 where it is also shown that the value of $\overline{D}$ differs by a factor of six for SWATH 6A between the strip theory and slender-body theory but less than a factor of two for SWATH 6D. The peak value of SWATH 6A is therefore caused by this change in the factor $\overline{D}$.

TABLE 2 - COMPARISON OF NUMERICAL VALUES OF PITCH DETERMINANT $\overline{D}$ FOR SWATH 6A AND 6D SHIPS USING SLENDER-BODY AND STRIP THEORIES

Quantities Needed to Calculate $\overline{D}$ (and Units)	SWATH 6A		SWATH 6D	
	Slender-Body Theory	Strip Theory	Slender-Body Theory	Strip Theory
L (m)	54.3		73.1	
M (kg-sec^2/m)	$0.2673.10^6$		$0.2917.10^6$	
C_{55} (kg-m)	$0.3483.10^9$		$0.9664.10^9$	
ω (1/sec)	0.0212		0.0183	
λ/L	1.25		0.96	
I (kg-m-sec^2)	$0.7825.10^8$		$1.0521.10^8$	
A_{55} (kg-m-sec^2)	$66.11.10^9$	$92.67.10^9$	$573.23.10^9$	$644.33.10^9$
B_{55} (kg-m-sec)	$0.1599.10^9$	$0.5994.10^9$	$0.8222.10^9$	$1.58.6.10^9$
$C_{55} - (I+A_{55})\omega^2$ (kg-m)	$-0.0508.10^8$	$-0.0685.10^8$	$-0.9537.10^8$	$-1.1918.10^8$
ωB_{55} (kg-m)	$0.0246.10^8$	$0.1271.10^8$	$0.1504-10^8$	$0.2894.10^8$
$\overline{D}$ (kg^2-m^2)	$0.3186.10^{14}$	$2.0847.10^{14}$	$0.9322.10^{16}$	$1.5041.10^{16}$

SUMMARY AND CONCLUSIONS

This report presents the application of the unified slender-body theory to predict the motion of SWATH ships in head seas. At zero speed, the computed results for a twin ellipsoid show overall improvement in the hydrodynamic forces and motions compared with three-dimensional theory. For SWATH ships with high forward speed in head seas and in following seas, there is some improvement in the added-mass and damping coefficients compared with two-dimensional results, but for the exciting forces and motions the same improvement is not expected. In following seas, the motions of SWATH 6A show unexpected large peak values at small encounter frequencies. The motion results of SWATH 6D agree very well with the experiments.

From the present study, the following conclusions have been drawn:

1. The slender-body theory improves the two-dimensional predictions of added-mass and damping coefficients. The same improvement has been shown for surface ships in Reference 5.

2. The application of the slender-body theory for the prediction of exciting forces has not been entirely successful. Further investigation is necessary in this area.

3. Except for the pitch motion of SWATH 6D in following seas, the computed motions have not been significantly improved by the application of the slender-body theory. When the sectional interaction terms are solved with the sectional source strength of the slender-body theory, they are strongly influenced by strip theory in head seas. Further investigation of these interactions is therefore warranted and is necessary to the final development of the slender-body theory.

ACKNOWLEDGMENT

The author gratefully acknowledges the support of Ms. M.D. Ochi, Dr. D.D. Moran, and Mr. V. Monacella.

REFERENCES

1. Lee, C.M., "Theoretical Prediction of Motion of Small-Waterplane-Area, Twin-Hull (SWATH) Ships in Waves," DTNSRDC Report 76-0046 (Dec 1976).

2. Hong, Y.S., "Improvements in the Prediction of Heave and Pitch Motion for SWATH Ships," DTNSRDC Dept. Rept. SPD-0928-02 (Apr 1980).

3. Salvesen, N., E.O. Tuck and O. Faltinsen, "Ship Motion and Seas Loads," Trans. SNAME, Vol. 78, pp. 250-287 (1970).

4. Newman, J.N., "The Theory of Ship Motion," Adv. in Appl. Mech., Vol. 18, pp. 221-283 (1978).

5. Newman, J.N. and P. Sclavounos, "The Unified Theory of Ship Motion," Proc. Thirteenth Symposium on Naval Hydrodynamics, Tokyo, Japan, p. 373 (Oct 1980).

6. Hong, Y.S., "Prediction of Motions of SWATH Ships in Following Seas," DTNSRDC Report 81/039 (Nov 1981).

7. Tuck, E.O., "The Steady Motion of a Slender Ship," Ph.D. thesis, University of Cambridge, Cambridge, England (1963).

8. Ursell, F., "On the Heaving Motion of a Circular Cylinder on the Surface of a Fluid," J. Mech. Appl. Math., Vol. 2, pp. 213-218 (1949).

9. Frank, W., "Oscillation of Cylinder in or below the Free Surface of Deep Fluids," DTNSRDC Report 2375 (1967); avail. DTNSRDC.

10. Wehausen, J.V. and E.V. Laitone, "Surface Waves," in Handbuch der Phys., Vol. 9, pp. 446-778 (1960).

11. Lighthill, M.J., "Fourier Analysis and Generalized Functions," The University Press, Cambridge, England (1970).

12. Hadamard, J., "Lectures on Cauchy's Problem in Linear Partial Differential Equations," Yale University Press (1932).

INITIAL DISTRIBUTION

Copies		Copies	
1	CHONR/432/C.M. Lee	4	U. of Cal/Dept Naval Arch, Berkeley
2	NRL		1 Eng Library
	1 Code 2027		1 Webster
	1 Code 2627		1 Paulling
			1 Wehausen
3	USNA	2	U. of Cal, San Diego
	1 Tech Lib		1 A.T. Ellis
	1 Nav Sys Eng Dept		1 Scripps Inst Lib
	1 Bhattacheryya		
2	NAVPGSCOL	2	CIT
	1 Library		1 Aero Lib
	1 Garrison		1 T.Y. Wu
1	NADC	1	Catholic U. of Amer/Civil & Mech Eng
1	NELC/Lib	1	Colorado State U./Eng Res Cen
2	NOSC	1	Florida Atlantic U.
	1 Library		1 Tech Lib
	1 Higdon		
1	NCEL/Code 131 Port Hueneme, CA 93043	1	U. of Hawaii/St. Denis
		1	U. of Illinois/J. Robertson
12	NAVSEA	2	U. of Iowa
	1 SEA 312/G. Kerr		1 Library
	1 SEA 3124/C. Kennel		1 Landweber
	1 SEA 31241/P. Chatterton		
	1 SEA 03R/L. Benen		
	1 SEA 03R/R. Dilts	1	U. of Kansas/Civil Eng Lib
	1 SEA 03R/N. Kobitz		
	1 SEA 03R/J. Schuler	1	Lehigh U./Fritz Eng Lab Lib
	1 SEA 312/P.A. Gale		
	1 SEA 3213/E.N. Comstock	5	MIT
	1 SEA 321/R.G. Keane, Jr.		1 Yeung
	1 SEA 3213/W. Livingston		1 Ogilvie
	1 SEA 61433/F. Prout		1 Abkowitz
			1 Newman
12	DTIC		1 Sclavounos
1	NSF/Engineering Lib	2	U. of Mich/NAME
			1 Library
1	DOT/Lib TAD-491.1		1 M. Parsons
1	NBS/Klebanoff	1	U. of Notre Dame
			1 Eng Lib
1	MARAD/Lib		

Copies	
2	New York U./Courant Inst
	1 A. Peters
	1 J. Stoker
4	SIT
	1 Breslin
	1 Savitsky
	1 Dalzell
	1 Kim
1	U. of Texas/Arl Lib
2	Southwest Res Inst
	1 Applied Mech Rev
	1 Abramson
1	Stanford Res Inst/Lib
2	U. of Washington
	1 Eng Lib
	1 Mech Eng/Adee
3	Webb Inst
	1 Library
	1 Lewis
	1 Ward
1	Woods Hole/Ocean Eng
1	SNAME/Tech Lib
1	Bethlehem Steel/New York/Lib
1	General Dynamics, EB/Boatwright
1	Gibbs & Cox/Tech Info
1	Hydronautics
	1 Library
1	Newport News Shipbuilding/Lib
1	Sperry Rand/Tech Lib
1	Sun Shipbuilding/Chief Naval Arch
2	American Bureau of Shipping
	1 Lib
	1 Cheng

Copies	
1	Maritime Research Information Service

CENTER DISTRIBUTION

Copies	Code	Name
1	1102	G.D. Elmer
1	117	R.M. Stevens
1	1170	G.R. Lamb
1	1500	W.B. Morgan
1	1504	V.J. Monacella
1	1506	S. Hawkins
1	1520	W.C. Lin
1	1520	E.N. Hubble
1	1521	W.G. Day
1	1521	A.M. Reed
1	1522	G.F. Dobay
1	1522	M.B. Wilson
1	1540	J.H. McCarthy
1	1540	B. Yim
1	1542	Branch Head
1	1560	D. Cieslowski
1	1561	G.C. Cox
1	1561	S.L. Bales
1	1561	E.A. Baitis
1	1561	W.R. McCreight
1	1562	D.D. Moran
1	1562	E.E. Zarnick
1	1562	K.K. McCreight
10	1562	Y.S. Hong
1	1563	W.E. Smith
1	1564	J.P. Feldman
1	1564	R.M. Curphey
30	5211.1	Reports Distribution
1	522.1	Unclassified Lib (C)
1	522.2	Unclassified Lib (A)

DTNSRDC ISSUES THREE TYPES OF REPORTS

1. DTNSRDC REPORTS, A FORMAL SERIES, CONTAIN INFORMATION OF PERMANENT TECHNICAL VALUE. THEY CARRY A CONSECUTIVE NUMERICAL IDENTIFICATION REGARDLESS OF THEIR CLASSIFICATION OR THE ORIGINATING DEPARTMENT.

2. DEPARTMENTAL REPORTS, A SEMIFORMAL SERIES, CONTAIN INFORMATION OF A PRELIMINARY, TEMPORARY, OR PROPRIETARY NATURE OR OF LIMITED INTEREST OR SIGNIFICANCE. THEY CARRY A DEPARTMENTAL ALPHANUMERICAL IDENTIFICATION.

3. TECHNICAL MEMORANDA, AN INFORMAL SERIES, CONTAIN TECHNICAL DOCUMENTATION OF LIMITED USE AND INTEREST. THEY ARE PRIMARILY WORKING PAPERS INTENDED FOR INTERNAL USE. THEY CARRY AN IDENTIFYING NUMBER WHICH INDICATES THEIR TYPE AND THE NUMERICAL CODE OF THE ORIGINATING DEPARTMENT. ANY DISTRIBUTION OUTSIDE DTNSRDC MUST BE APPROVED BY THE HEAD OF THE ORIGINATING DEPARTMENT ON A CASE-BY-CASE BASIS.